High-resolution coincidence counting system
for large-scale photonics applications

Josef Hloušek[©],[*] Jan Grygar[©], Michal Dudka[©], and Miroslav Ježek[©][†]

Department of Optics, Faculty of Science, Palacký University, 17 listopadu 12, Olomouc 77900, Czech Republic

The increasing complexity of recent photonic experiments challenges the development of efficient multichannel coincidence counting systems with high-level functionality. Here, we report a coincidence unit able to count detection events ranging from single to 16-fold coincidences with full channel-number resolution. The device operates within sub-100-ps coincidence time windows, with a maximum input frequency of 1.5 GHz and an overall jitter of less than 10 ps. The unit high-level timing performance renders it suitable for quantum photonic experiments employing low-timing-jitter single-photon detectors. Additionally, the unit can be used in complex photonic systems to drive feed-forward loops. We demonstrate the developed coincidence counting unit in photon-number-resolving detection to directly quantify the statistical properties of light, specifically coherent and thermal states, with a fidelity exceeding 0.999 up to 60 photons.

I. INTRODUCTION

A coincidence counting unit (CCU) is an essential tool widely employed in all applications requiring the detection of a large number of photons (or other particles) and processing of the detected signals. Modern quantum experiments employ increasingly complex systems with a growing number of input and output channels [1–3]. These large-scale photonics systems hinge on the ability to generate, control, and analyze the multiphoton quantum states [1,4–6] frequently used in quantum communications [7,8], quantum computation, and simulations [9]. Particularly, complex coincidence processing has become an integral part of measuring unknown optical states by photon-number-resolving detectors based on multiplexing [10–12]. Detected statistical properties of light are routinely applied to quantify nonclassicality and quantum non-Gaussianity [13–17]. Furthermore, the advanced functionality of these devices is of considerable interest in on-the-fly multifold coincidence analysis to control large-scale quantum systems via feed-forward operation and photon-number-resolving postselection [18,19].

Conventional approaches to detect coincidences are (1) time-to-amplitude converter (TAC) together with a single- or multichannel analyzer, (2) time-to-digital converter (TDC) followed by postprocessing, and (3) overlap logic coincidence systems realized with discrete components or using a field-programmable gate array (FPGA). TACs and TDCs both typically offer tens-of-picosecond resolution. TACs are not easily scaled up for multicoincidence systems and possess a considerable dead time limiting rate throughput to tens of thousands of events per second [20,21]. TDC-based solutions stream time tags to a computer for further processing. Therefore, a large amount of data are processed offline. Alternatively, TDCs are combined with an FPGA for subsequent processing [22]. Pulse overlap coincidence systems use fast logic gates and multiplexers to capture detection events and detect coincidences [21]. Coincidence counting and histogramming could be programmed into a microcontroller [23] or FPGA [24]. Functional blocks such as internal delay lines, coincidence counters, and a processor can all be integrated within a single FPGA chip [25–28]. Lately, multichannel TDC-based coincidence counter architecture in the same FPGA chip was introduced [29].

In this paper, we report an ultrafast electronic multichannel CCU, producing a histogram of all possible coincidence events for up to 16 constituent detectors. The device performs a real-time classification of all possible detection events in a 2^{16}-element histogram with a rate of up to 3 million events per second. We have conducted a comprehensive characterization of the presented CCU, revealing excellent performance parameters, including a sub-100-ps coincidence window, sub-10-ps jitter, and an ultralow coincidence error probability. Furthermore, we demonstrate the CCU versatility by implementing a multiphoton counting experiment to fully characterize the statistical properties of incident light.

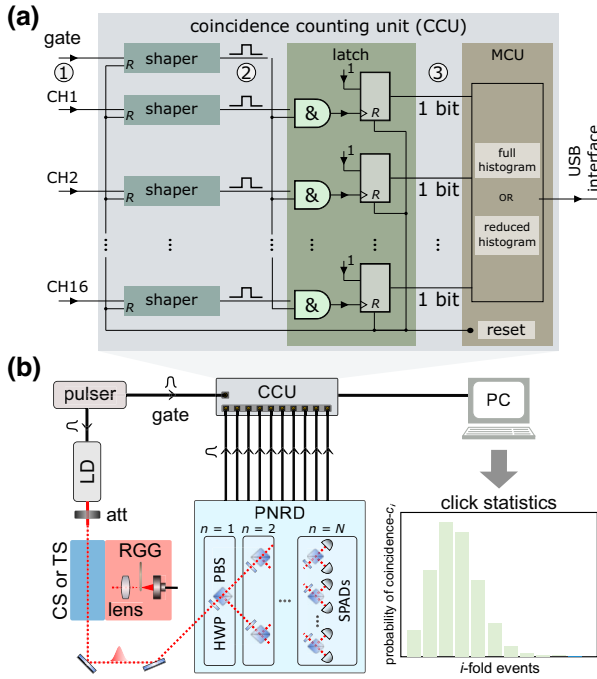*hlousek@optics.upol.cz
†jezek@optics.upol.cz

FIG. 1. (a) A block diagram of the CCU: the shapers prepare square pulses; coincidences are evaluated as an overlap (&) of the pulses and can be directly used or counted and sorted in histograms by the microcontroller unit (MCU). (b) For photon-number-resolved detection (PNRD), the CCU is connected to a spatial-multiplexed optical network consisting of tunable beam splitters and SPADs. The resulting coincidence histogram allows for statistical analysis of the incident signal.

II. COINCIDENCE COUNTING UNIT

Figure 1(a) shows an overview of the CCU architecture based on fast positive emitter-coupled logic (ECL) offering high-resolution coincidence counting. The CCU consists of input signal overlap logic and data processing unit. The device accepts 16 data inputs and a single gate input and yields the complete histogram of 2^{16} multicoincidences of the inputs within the gate signal. Each input channel contains a shaping circuit with high-resolution programmable delay lines to detect an input signal edge and provides the output ECL pulse of a given width and delay. The pulse width corresponds to half of the coincidence window, which can be tuned independently for each channel. After the signal shaping, the signal and gate pulse enable inputs of ECL latch circuitry. The latch records the overlap of individual signal pulses and the gate signal and stores information about coincidence events and single-channel pulses. Data from the latch are transferred in the form of bits. A detailed description of the pulse shaping and processing is presented in Appendix A.

The outputs of the latch can be directly employed for implementing real-time feed-forward control. For example, one can switch between states of an electro-optic

modulator to modify the performance of the following experimental setup. The maximum input frequency is limited to 1.5 GHz by the maximum operating frequency of the delay lines. When a higher voltage is required to control the subsequent devices, it is necessary to utilize a logic-level translator. In this work, we use a microcontroller unit for controlling and monitoring overlap logic and data processing and storage. Consequently, an ECL-CMOS translator is required, reducing the maximum input frequency to 800 MHz.

The presented CCU allows the operation of two specific regimes depending on the complexity of the measurement. One can store the complete information about all possible coincidence events ($2^{16} = 65\,536$ kinds of coincidence events in total), termed the full histogram regime. In the second regime, the CCU counts only coincidences of the same order without information about the channel number (the reduced histogram regime). For our specific technical solution, the maximum processing rate is about 3 million events per second for the reduced histogram and 2 million events for the full histogram. This rate can be further enhanced by utilizing an FPGA.

Another purpose of the microcontroller unit is to configure the delay lines in the shapers to synchronize the input signals and set the length of the coincidence window. It also enables self-calibration of the CCU and monitoring of the operating temperature and other parameters. The minimum coincidence window can be set below 100 ps, and the maximum coincidence window length can reach 20 ns. The detailed electronic characterization of the CCU is presented in Appendix B. A comparison with the state-of-the-art approaches is given in Appendix C.

III. PHOTON STATISTICS MEASUREMENT OF LARGE OPTICAL STATES

Numerous technological approaches have been developed and experimentally verified to achieve photon-number resolution, falling into two categories: inherent photon-number resolution (superconducting nanowire single-photon detectors [30–32] or transition edge sensors [33–38]) and multiplex and/or multipixel detection schemes [10–17,39–51]. In our case, the multiplexed detector consists of tunable beam splitters composed of a half-wave plate and a polarizing beam splitter; see Fig. 1(b). This beam-splitting approach allows accurate adjustments of the splitting ratio with an absolute error below 0.3%. Each channel is coupled to a multimode fiber and brought to a single-photon avalanche diode (SPAD) with efficiency ranging from 55% to 70% at 0.8 μm, 200–300 ps timing jitter, and 20–30 ns dead time. The total detection efficiency η is defined as the ratio of the total number of detected photons to the total number of incident photons. Based on the measured transmittance of the multiport optical network and SPAD efficiencies,

we experimentally determined η as 50(1)%. Furthermore, utilizing low-loss optics and superconducting nanowire single-photon detectors [52] can enhance global efficiency to over 85%.

As a light source, we use a gain-switched semiconductor laser diode to generate a coherent nanosecond pulsed light with a central wavelength of 0.8 μm. The laser diode is driven by nanosecond electronic pulses at a repetition rate of 1 MHz. We use the temporal intensity modulation of the initial coherent light by rotating ground glass to generate pseudothermal light with Bose-Einstein distribution [53]. The optical signal is collected by a single-mode fiber to produce a single-mode thermal state.

We quantify the statistical properties of light, focusing on coherent and thermal states, across a wide range of mean photon numbers. These states of light are detected by a ten-channel multiplexed detector and processed by the CCU in the reduced histogram regime. The coincidence window width is set to be significantly larger than both the optical pulse width and the detector jitter. Due to nonunity detection efficiency, noise, and a finite number of single-photon detection channels, we observe the probability distribution of the coincidence events (i.e., click statistics) c_m instead of the photon statistics p_n. However, the click statistics still carry information about the character of the initial state of light. The parameter quantifying this phenomenon is called the binomial parameter [11,54] defined as $Q_b = \frac{\langle (\Delta c)^2 \rangle}{\frac{\langle c \rangle}{N}\left(1 - \frac{\langle c \rangle}{N}\right)} - 1$, where $\langle c \rangle = \sum_{i=0}^{N} i c_i$, $\langle (\Delta c)^2 \rangle = \sum_{i=0}^{N}(i - \langle c \rangle)^2 c_i$, and N stands for the number of detection channels. States of light with a Poisson distribution result in a binomial parameter of $Q_b = 0$, whereas non-negative values occur for super-Poissonian states (see Fig. 2). For coherent states, we measure the binomial parameters that vary between $1(5) \times 10^{-4}$ and $1.0(5) \times 10^{-3}$, with a mean number of clicks $\langle c \rangle$ ranging from 0.005 to 5. The values of the binomial parameter do not exactly match zero due to the higher variance in the measured click statistics caused
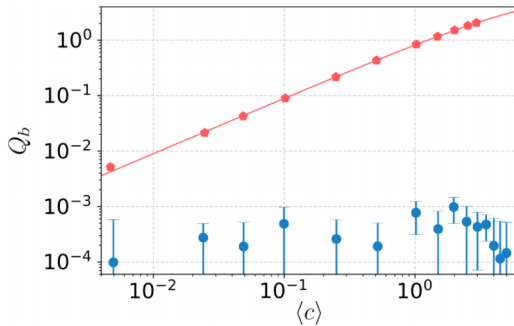

FIG. 2. The binomial parameter Q_b as a function of the mean number of clicks $\langle c \rangle$. Shown are the coherent states (blue circles) and thermal states (red pentagons); the solid line represents the theoretical model for thermal state.
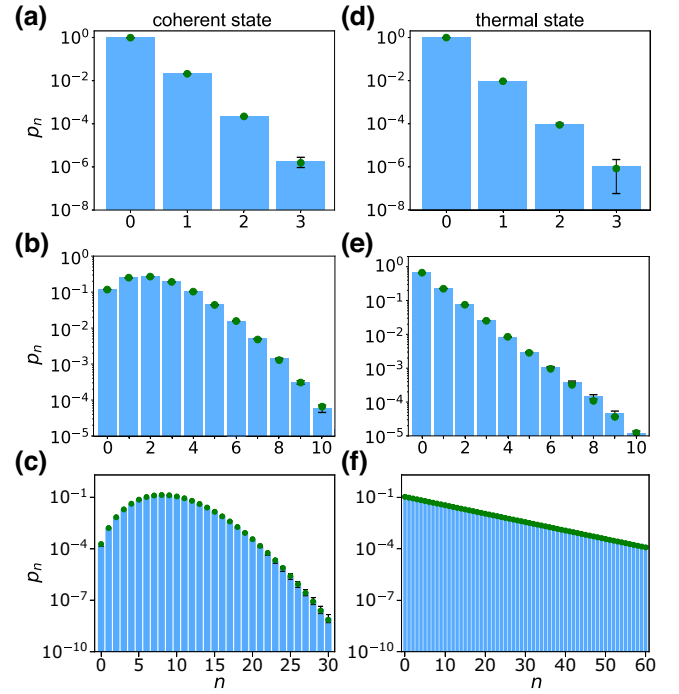

FIG. 3. Retrieved (blue bars) and theoretical (green circles) photon statistics of coherent state (a)–(c) and thermal state (d)–(f) for several mean photon numbers: (a) $\langle n \rangle_{CS} = 0.02119(3)$, (b) $\langle n \rangle_{CS} = 2.144(3)$, (c) $\langle n \rangle_{CS} = 10.21(1)$, (d) $\langle n \rangle_{TS} = 0.00949(5)$, (e) $\langle n \rangle_{TS} = 0.5113(4)$, and (f) $\langle n \rangle_{TS} = 8.41(3)$.

by excess noise in the light source. Measured thermal states cover values of mean number of clicks $\langle c \rangle$ ranging from 0.002 to 3 with Q_b that encompasses the range from $5.1(7) \times 10^{-3}$ to 2.060(1). All measured values exhibit excellent agreement with the theoretical predictions.

In addition to directly measuring the click statistics, we have also retrieved photon statistics. Here, we demonstrate the faithful photon statistics reconstruction over three orders of magnitude of the mean photon numbers within a dynamic range of up to 60 photons (see Fig. 3). Results show unprecedented agreement between theoretical distributions (green circles) and observed data (blue bars) down to probabilities of 10^{-8}. It is important to stress here that the photon statistics retrieval includes all imperfections, such as slight imbalances of splitting ratios in the photon-number-resolving detector and imperfect light-state preparation. The fidelity of the retrieved photon statistics, defined as $\mathcal{F} = \left(\sum_{n=0}^{n_{max}} \sqrt{p_n p_n^{ideal}}\right)^2$, surpasses 0.999 for all measured states of light [see Fig. 4(a)]. In fact, coherent states exhibit a fidelity exceeding 0.9997. As the mean photon number increases, the retrieval process degrades. This is a result of the increased probability of higher Fock states within the analyzed state, leading to a progressive divergence from the detector dynamic range.
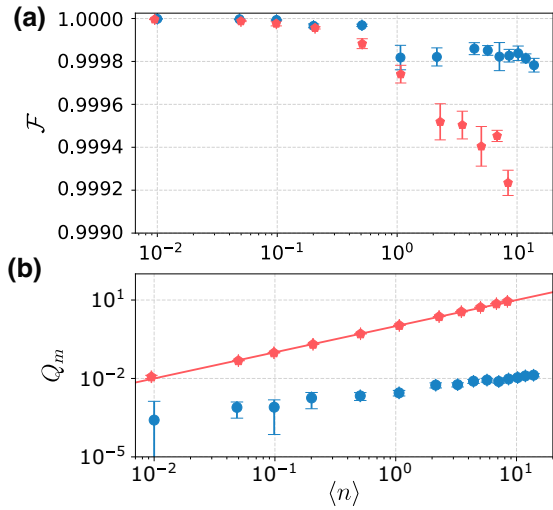
FIG. 4. Quantification of the retrieved photon statistics p_n: (a) fidelity $\mathcal{F}$ and (b) Mandel parameter Q_m as a function of mean photon number $\langle n \rangle$. Shown are the coherent states (blue circles) and thermal states (red pentagons); the solid line represents the theoretical model for thermal state.

The extent of measurement degradation by the reconstruction error naturally depends on the photon statistics of the initial light state.

The presented measurement workflow is scalable with the total number of detection channels. Increasing their quantity can expand the detector dynamic range, enabling the measurement of optical states with even higher intensities. Also, the presented reconfigurable detection network allows for a decrease in the number of employed detectors to measure specific characteristics of the source under test. Specifically, this enables a direct evaluation of the anticorrelation parameter α [55], nonclassicality [14,15,17,54], and quantum non-Gaussianity [16,56].

With a knowledge of the photon statistics, we explore the Mandel parameter [13,57,58], which is a convenient way to characterize deviation from Poisson statistics. The Mandel parameter is defined as the ratio of the second and first moments of photon statistic distribution: $Q_m = (\langle(\Delta n)^2\rangle - \langle n \rangle)/\langle n \rangle$. We calculate the Mandel parameter of the retrieved photon statistics as a function of the mean photon number of the initial state; see Fig. 4(b). We measure coherent states with Poisson statistics with the Mandel parameter Q_m ranging from $3(5) \times 10^{-4}$ to $1.3(2) \times 10^{-2}$ and the mean photon number reaching $\langle n \rangle = 19.84(2)$. The ideal Poisson distribution with photon number variance $\langle(\Delta n)^2\rangle = \langle n \rangle$ reaches the Mandel parameter $Q_m = 0$. The measured data are influenced by excess noise, leading to a slight offset from the anticipated value of the Mandel parameter. For generated pseudothermal states, we obtain the Mandel parameter ranging from $Q_m = 0.012(2)$ to $8.93(3)$ for $\langle n \rangle$ up to $8.410(3)$. The ideal chaotic thermal light exhibits photon bunching, with the Mandel parameter

Q_m equaling the mean photon number $\langle n \rangle$, as confirmed by the data [see Fig. 4(b)].

IV. CONCLUSION

We designed and developed a high-performance CCU, achieving low propagation delay, a well-defined adjustable coincidence window, 10-ps overall jitter, and high-precision multicoincidence counting. The CCU enables storing the complete histograms of all possible coincidence events (65 536 for 16 channels) with full channel resolution or a reduced histogram carrying information only about summarized n-fold coincidences. Alternatively, the information about the coincidence events can be directly used as an advanced trigger to control complex photonic systems. In terms of scalability, the CCU supports extensions of the total number of input channels, easily exceeding 100. Advancements in coincidence counting and processing to a mesoscopic scale offer groundbreaking applications in quantum communications, simulations, and boson sampling machines.

The presented CCU allows for a wide range of multiple-detector experiments. We performed a photon-number counting experiment employing single-photon detectors to investigate the statistical properties of the initial light. The results show unprecedented accuracy of photon statistics measurement ($\mathcal{F} > 0.999$) with a dynamic range of photon-number resolution up to 60 photons. The presented measurement process is independent of the number of channels and can be scaled up to a level where hundreds of photons can be detected, which is crucial for quantum receivers, quantum tomography, photonic source benchmarking, and other applications.

APPENDIX A: ELECTRONIC DESIGN AND IMPLEMENTATION OF THE COINCIDENCE COUNTING SYSTEM

Here, we present a detailed description of the developed ultrafast electronic multichannel CCU based on ECL circuitry. In the main text, Fig. 1(a) shows an overview of the CCU architecture consisting of a shaper, latch, and microcontroller. A shaper is a crucial circuit building block comprised of a fast comparator (MAX 9600), a pair of delay lines (SY89295U or MC100EP195, depending on market availability), and basic gates (MC100EP05). Figure 5(a) depicts a block diagram of a single shaper. For a detailed pulse shaping and processing description, see Fig. 5(b). The fast comparator processes the input signal to
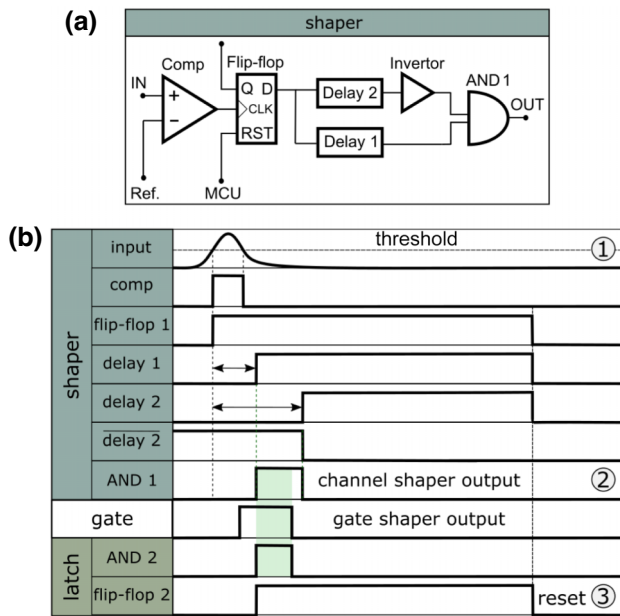
FIG. 5. (a) A block diagram of a shaper and (b) the timing diagram of the signal processing.

convert it from the original waveform to a defined pulse, triggering the first flip-flop circuit. Each input channel has an adjustable threshold from 1 to 4 V. The flip-flop stores state information and creates a time window independent of the input signal. The flip-flop output is split into two pulses and modified by parallel delay lines and inverters.

The pulse emitted by the shaper is defined as an output of the AND gate that implements the logical conjunction of the delayed pulses. The first (second) delay line sets the rising (falling) edge of the corresponding time window. The width of the time window is given as the time difference between these two propagation delays. The gate signal has its shaper, including one extra delay line for additional delay adjustment. The gate pulse is distributed to individual latch inputs utilizing electronic repeaters. Recently, after acquiring data for this work, we updated the CCU design. We distribute the rising edges of the gating signal and subsequently generate individual gate pulses. This approach mitigates spreading of short edges due to long propagation on printed circuit boards and further improves the quality (steepness) of the rising and falling edges.

Each programmable delay line employed in the shaping circuitry has 1024 discrete steps with an average delay of 9 ps (for our setting and operating temperature). The resulting coincidence window is adjustable from the sub-100-ps regime to approximately 20 ns, i.e., two times the maximum delay of a single signal shaper. The delay lines can also compensate for differences in input signal arrival times. The individual channels can be delayed within a range of up to 10 ns, as discussed above. The maximum delay between the gate and the signal channels can be set to 20 ns for a sub-100-ps coincidence window. However, for the maximum 20-ns coincidence window, the entire capacity of the delay lines is used to create the coincidence window, and the input signals need to be externally synchronized.

The latch, composed of 16 AND gates and the flip-flop circuits (MC100EP51), counts all possible coincidences between the rising edge of the gate pulse and 16 rising edges of the signal pulses. The AND gates generate an output pulse only when input and gate pulses are received simultaneously. The microcontroller unit (STM32F429) receives the data from the latch and sorts the results into a histogram in memory. Data, including information about the number of single-channel pulses and coincidences, are transferred to a personal computer via USB. Finally, the microcontroller unit resets all flip-flop circuits and enables the CCU for another detection event. Our CCU design offers unparalleled scalability, accommodating an unlimited number of input channels with the potential to support up to 100 input channels.

APPENDIX B: ELECTRONIC CHARACTERIZATION OF THE COINCIDENCE COUNTING SYSTEM

To characterize the performance and capabilities of the presented device, we evaluate the following figures of merit: (1) the minimum and maximum coincidence window length, (2) timing granularity, (3) timing jitter, (4) higher-order coincidence failure probability, and (5) maximum detection rate. We analyze the coincidence window width and rising and falling edges. The whole measurement is based on changing the mutual position of the gate and channel pulse. As a result, we obtain the number of coincidence events as a function of time delay. The minimum and maximum widths of the coincidence window are sub-100 ps and 20 ns, respectively. The main limitation of the maximum coincidence window width is the maximum range of delay lines. The results show that the coincidence windows are well defined in time, and they are almost perfectly rectangular with sharp edges with a value typically around 18(5) ps for all channels (see Figs. 6 and 7). The employed high-speed ECL components with fast transition times guarantee a short propagation delay below 5 ns. The overall jitter of the presented CCU is less than 10 ps.

The presented CCU meets the conditions for a high-resolution coincidence system with equal probabilities for all orders of coincidence events. We have analyzed the precision of counting coincidences utilizing a home-built multichannel pulse generator with a repetition rate from 0.2 to 10 MHz. The signal is generated by a relaxation oscillator whose output is delayed by a resistor-capacitor low-pass network and fast inverter with Schmitt trigger inputs (74ACT14T). This generator was developed to simulate the typical output signals of state-of-the-art
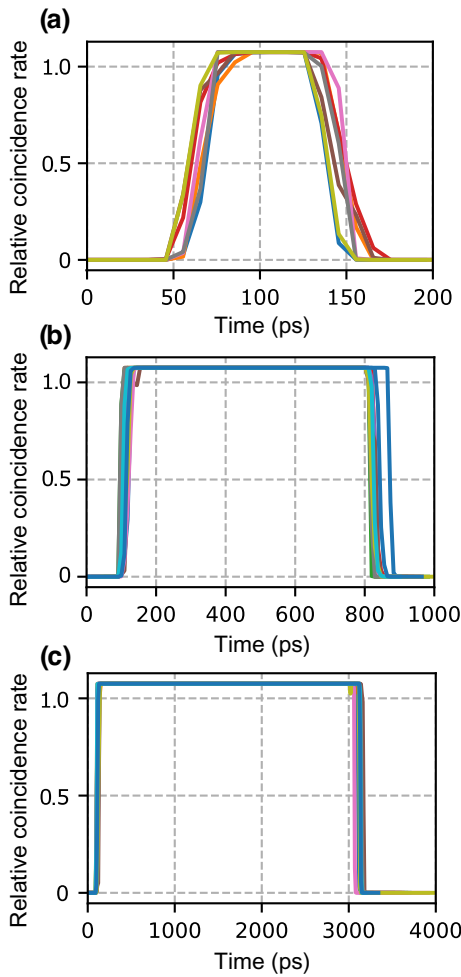
FIG. 6. A full scan of the coincidence window of width (a) sub-100 ps, (b) 700 ps, and (c) 3 ns.

single-photon detectors with a jitter of less than 10 ps. All detection channels are synchronized with the generator output pulse. The result is that all coincidence events
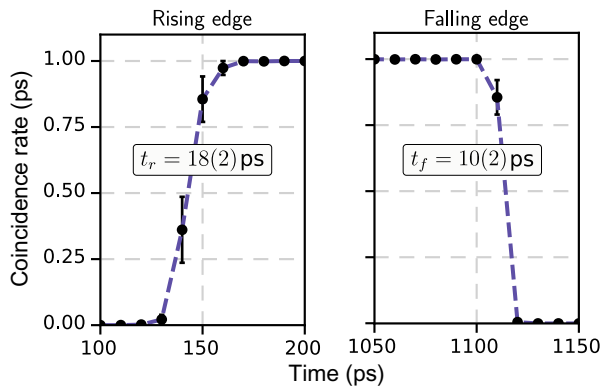

FIG. 7. The typical achieved rising and falling edges (10%–90%) of the coincidence window (width: 1 ns). Presented values are calculated as the average over the 250 measurement runs. The error bars represent one standard deviation.
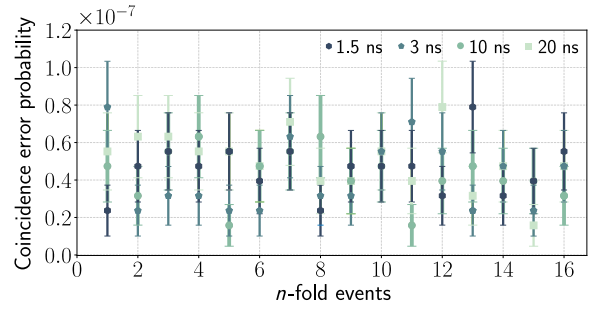

FIG. 8. Analysis of the coincidence error probability of the individual *n*-fold coincidences for several different widths of the coincidence windows: 1.5, 3.0, 10, and 20 ns. Presented values are calculated as the average over the 250 measurement runs. The error bars represent one standard deviation.

should be evaluated as 16-fold coincidences. We compare the measured coincidence events with the number of gating pulses to evaluate the counting error of the number of coincidence events. For measurements ranging from 16-fold coincidences down to single events, we systematically deactivate the detection channels one by one. Figure 8 shows the analysis of coincidence counting precision for several configurations of coincidence window width from 1.5 up to 20 ns. All coincidence errors across all tested coincidence windows are lower than 10^{-7}. This indicates ultralow coincidence errors due to resetting the latches, most probably caused by back reflections via imperfect impedance matching.

TABLE I. Performance parameters comparison of the presented CCU and other coincidence unit approaches.

Ref.	[25]	[26]	[27]	[28]	[29]	[59]	This work
Number of channels	8	48	8	32	8	20	16
Measurable coincidence folds	8	6	8	8	8	20	16
Maximum input frequency (MHz)	163	76	50	80	40[a]	400[b]	1500
Minimum coincidence window (ns)	0.47	0.3	10	0.39	⋯	0.46	<0.1
Maximum coincidence window (ns)	13.22	1.9	70	⋯	⋯	10	20
Channel resolution	No	No	No	No	Yes	No	Yes

[a]Up to 2-fold coincidences only.
[b]Characterized in 2-fold coincidence measurement.

APPENDIX C: CCU PERFORMANCE COMPARISON

In Table I, a summary of the performance of the various CCU approaches is shown. The presented CCU offers high n-fold coincidence counting ($n = 16$) with channel-number resolution, the shortest well-defined sub-100-ps coincidence windows with 10-ps overall jitter, and the highest maximum input frequency of 1.5 GHz.

———————————

[1] J. Wang, S. Paesani, Y. Ding, R. Santagati, P. Skrzypczyk, A. Salavrakos, J. Tura, R. Augusiak, L. Mančinska, D. Bacco, D. Bonneau, J. W. Silverstone, Q. Gong, A. Acín, K. Rottwitt, L. K. Oxenløwe, J. L. O'Brien, A. Laing, and M. G. Thompson, Multidimensional quantum entanglement with large-scale integrated optics, Science **360,** 6386 (2018).

[2] H. Wang, J. Qin, X. Ding, M.-C. Chen, S. Chen, X. You, Y.-M. He, X. Jiang, L. You, Z. Wang, C. Schneider, J. J. Renema, S. Höfling, C.-Y. Lu, and J.-W. Pan, Boson sampling with 20 input photons and a 60-mode interferometer in a 10^{14}-dimensional Hilbert space, Phys. Rev. Lett **123,** 25 (2019).

[3] H.-S. Zhong *et al.*, Quantum computational advantage using photons, Science **370,** 6523 (2020).

[4] X.-C. Yao, T.-X. Wang, P. Xu, H. Lu, G.-S. Pan, X.-H. Bao, C.-Z. Peng, C.-Y. Lu, Y.-A. Chen, and J.-W. Pan, Observation of eight-photon entanglement, Nat. Phot. **6,** 225 (2012).

[5] X.-L. Wang, L.-K. Chen, W. Li, H.-L. Huang, C. Liu, C. Chen, Y.-H. Luo, Z.-E. Su, D. Wu, Z.-D. Li, H. Lu, Y. Hu, X. Jiang, C.-Z. Peng, L. Li, N.-L. Liu, Y.-A. Chen, C.-Y. Lu, and J.-W. Pan, Experimental ten-photon entanglement, Phys. Rev. Lett **117,** 21 (2016).

[6] S. Paesani, Y. Ding, R. Santagati, L. Chakhmakhchyan, C. Vigliar, K. Rottwitt, L. K. Oxenløwe, J. Wang, M. G. Thompson, and A. Laing, Generation and sampling of quantum states of light in a silicon chip, Nat. Phys. **15,** 9 (2019).

[7] S. Aaronson and A. Arkhipov, in *Quantum Information and Measurement 2014* (Optica Publishing Group, Messe Berlin, Berlin Germany, 2014).

[8] S. Pirandola, U. L. Andersen, L. Banchi, M. Berta, D. Bunandar, R. Colbeck, D. Englund, T. Gehring, C. Lupo, C. Ottaviani, J. L. Pereira, M. Razavi, J. Shamsul Shaari, M. Tomamichel, V. C. Usenko, G. Vallone, P. Villoresi, and P. Wallden, Advances in quantum cryptography, Adv. Opt. Photonics **12,** 1012 (2020).

[9] A. Aspuru-Guzik and P. Walther, Photonic quantum simulators, Nat. Phys. **8,** 4 (2012).

[10] H. Paul, P. Törmä, T. Kiss, and I. Jex, Photon chopping: New way to measure the quantum state of light, Phys. Rev. Lett **76,** 14 (1996).

[11] J. Sperling, W. Vogel, and G. S. Agarwal, True photocounting statistics of multiple on-off detectors, Phys. Rev. A **85,** 2 (2012).

[12] J. Hloušek, M. Dudka, I. Straka, and M. Ježek, Accurate detection of arbitrary photon statistics, Phys. Rev. Lett. **123,** 15 (2019).

[13] H. J. Kimble, M. Dagenais, and L. Mandel, Photon antibunching in resonance fluorescence, Phys. Rev. Lett. **39,** 11 (1977).

[14] H. Esat Kondakci, A. Szameit, A. F. Abouraddy, D. N. Christodoulides, and B. E. A. Saleh, Sub-thermal to super-thermal light statistics from a disordered lattice via deterministic control of excitation symmetry, Optica **3,** 5 (2016).

[15] J. Sperling, A. Eckstein, W. R. Clements, M. Moore, J. J. Renema, W. S. Kolthammer, S. W. Nam, A. Lita, T. Gerrits, I. A. Walmsley, G. S. Agarwal, and W. Vogel, Identification of nonclassical properties of light with multiplexing layouts, Phys. Rev. A **96,** 1 (2017).

[16] I. Straka, L. Lachman, J. Hloušek, M. Miková, M. Mičuda, M. Ježek, and R. Filip, Quantum non-Gaussian multiphoton light, Npj Quantum Inf. **4,** 1 (2018).

[17] M. Bohmann, L. Qi, W. Vogel, and M. Chekhova, Detection-device-independent verification of nonclassical light, Phys. Rev. Res. **1,** 3 (2019).

[18] V. Švarc, M. Nováková, G. Mazin, and M. Ježek, Fully tunable and switchable coupler for photonic routing in quantum detection and modulation, Opt. Lett. **44,** 5844 (2019).

[19] G. Luiz Zanin, M. J. Jacquet, M. Spagnolo, P. Schiansky, I. A. Calafell, L. A. Rozema, and P. Walther, Fiber-compatible photonic feed-forward with 99% fidelity, Opt. Express **29,** 3425 (2021).

[20] M. Beck, Comparing measurements of $g^{(2)}(0)$ performed with different coincidence detection techniques, J. Opt. Soc. Am. B **24,** 12 (2007).

[21] D. Branning, S. Bhandari, and M. Beck, Low-cost coincidence-counting electronics for undergraduate quantum optics, Am. J. Phys. **77,** 7 (2009).

[22] M. Wahl, T. Röhlicke, H.-J. Rahn, R. Erdmann, G. Kell, A. Ahlrichs, M. Kernbach, A. W. Schell, and O. Benson, Integrated multichannel photon timing instrument with very short dead time and high throughput, Rev. Sci. Instrum. **84,** 4 (2013).

[23] S. Gaertner, H. Weinfurter, and C. Kurtsiefer, Fast and compact multichannel photon coincidence unit for quantum information processing, Rev. Sci. Instrum. **76,** 12 (2005).

[24] D. Branning, S. Khanal, Y. H. Shin, B. Clary, and M. Beck, Note: Scalable multiphoton coincidence-counting electronics, Rev. Sci. Instrum. **82,** 1 (2011).

[25] B. K. Park, Y.-S. Kim, O. Kwon, S.-W. Han, and S. Moon, High-performance reconfigurable coincidence counting unit based on a field programmable gate array, Appl. Opt. **54,** 15 (2015).

[26] C. Zhang, W. Li, Y. Hu, T. Yang, G. Jin, and X. Jiang, 48-channel coincidence counting system for multiphoton experiment, Rev. Sci. Instrum. **87,** 11 (2016).

[27] A. K. Gupta, R. Sankara Prasad, L. Srivani, D. Thirugnana Murthy, B. K. Panigrahi, and G. Raghavan, in *2018 IEEE International Conference on Electronics, Computing and Communication Technologies (CONECCT)* (Institute of Electrical and Electronics Engineers (IEEE), Bangalore, India, 2018), p. 1.

[28] W. Li, Y. Hu, H.-s. Zhong, Y.-f. Wang, X.-l. Wang, C.-z. Peng, and X. Jiang, Time-tagged coincidence counting unit for large-scale photonic quantum computing, Rev. Sci. Instrum. **89**, 10 (2018).

[29] E. Arabul, S. Paesani, S. Tancock, J. Rarity, and N. Dahnoun, A precise high count-rate FGPA based multi-channel coincidence counting system for quantum photonics applications, IEEE Photonics J. **12**, 2 (2020).

[30] C. Cahall, K. L. Nicolich, N. T. Islam, G. P. Lafyatis, A. J. Miller, D. J. Gauthier, and J. Kim, Multi-photon detection using a conventional superconducting nanowire single-photon detector, Optica **4**, 1534 (2017).

[31] D. Zhu, M. Colangelo, C. Chen, B. A. Korzh, F. N. C. Wong, M. D. Shaw, and K. K. Berggren, Resolving photon numbers using a superconducting nanowire with impedance-matching taper, Nano Lett. **20**, 3858 (2020).

[32] X. Tao, H. Hao, X. Li, S. Chen, L. Wang, X. Tu, X. Jia, L. Zhang, Q. Zhao, L. Kang, and P. Wu, Characterize the speed of a photon-number-resolving superconducting nanowire detector, IEEE Photonics J. **12**, 1 (2020).

[33] A. E. Lita, A. J. Miller, and S. W. Nam, Counting near-infrared single-photons with 95% efficiency, Opt. Express **16**, 3032 (2008).

[34] T. Gerrits, B. Calkins, N. Tomlin, A. E. Lita, A. Migdall, R. Mirin, and S. W. Nam, Extending single-photon optimized superconducting transition edge sensors beyond the single-photon counting regime, Opt. Express **20**, 23798 (2012).

[35] L. A. Morais, T. Weinhold, M. P. de Almeida, J. Combes, A. Lita, T. Gerrits, S. W. Nam, A. G. White, and G. Gillett, Precisely determining photon-number in real-time, arXiv:2012.10158 [physics.ins-det] (2022).

[36] M. Eaton, A. Hossameldin, R. J. Birrittella, P. M. Alsing, C. C. Gerry, H. Dong, C. Cuevas, and O. Pfister, Resolution of 100 photons and quantum generation of unbiased random numbers, Nat. Photonics **17**, 106 (2022).

[37] R. Cheng, Y. Zhou, S. Wang, M. Shen, T. Taher, and H. X. Tang, A 100-pixel photon-number-resolving detector unveiling photon statistics, Nat. Photonics **17**, 112 (2022).

[38] P. Li, J. Zhong, W. Zhang, Z. Wang, Q. Ma, Z. Feng, W. Miao, Y. Ren, J. Li, Q. Yao, and S. Shi, High-performance Ti transition-edge sensor-based photon-number resolving detectors, J. Low. Temp. Phys. (2023).

[39] P. Kok and S. L. Braunstein, Detection devices in entanglement-based optical state preparation, Phys. Rev. A **63**, 3 (2001).

[40] J. Řeháček, Z. Hradil, O. Haderka, J. Peřina, and M. Hamar, Multiple-photon resolving fiber-loop detector, Phys. Rev. A **67**, 6 (2003).

[41] K. Banaszek and I. A. Walmsley, Photon counting with a loop detector, Opt. Lett. **28**, 1 (2003).

[42] M. J. Fitch, B. C. Jacobs, T. B. Pittman, and J. D. Franson, Photon-number resolution using time-multiplexed single-photon detectors, Phys. Rev. A **68**, 4 (2003).

[43] D. Achilles, C. Silberhorn, C. Śliwa, K. Banaszek, and I. A. Walmsley, Fiber-assisted detection with photon number resolution, Opt. Lett. **28**, 23 (2003).

[44] D. Achilles, C. Silberhorn, C. Sliwa, K. Banaszek, I. A. Walmsley, M. J. Fitch, B. C. Jacobs, T. B. Pittman, and J. D. Franson, Photon-number-resolving detection using time-multiplexing, J. Mod. Opt. **51**, 9 (2004).

[45] G. A. P. Thé and R. Viana Ramos, Multiple-photon number resolving detector using fibre ring and single-photon detector, J. Mod. Opt. **54**, 8 (2007).

[46] R. Kruse, J. Tiedau, T. J. Bartley, S. Barkhofen, and C. Silberhorn, Limits of the time-multiplexed photon-counting method, Phys. Rev. A **95**, 2 (2017).

[47] M. Mičuda, O. Haderka, and M. Ježek, High-efficiency photon-number-resolving multichannel detector, Phys. Rev. A **78**, 2 (2008).

[48] E. A. Dauler, A. J. Kerman, B. S. Robinson, J. K. Yang, B. Voronov, G. Goltsman, S. A. Hamilton, and K. K. Berggren, Photon-number-resolution with sub-30-ps timing using multi-element superconducting nanowire single photon detectors, J. Mod. Opt. **56**, 2 (2009).

[49] T. J. Bartley, G. Donati, X.-M. Jin, A. Datta, M. Barbieri, and I. A. Walmsley, Direct observation of sub-binomial light, Phys. Rev. Lett **110**, 17 (2013).

[50] X. Chen, C. Ding, H. Pan, K. Huang, J. Laurat, G. Wu, and E. Wu, Temporal and spatial multiplexed infrared single-photon counter based on high-speed avalanche photodiode, Sci. Rep. **7**, 1 (2017).

[51] J. Tiedau, E. Meyer-Scott, T. Nitsche, S. Barkhofen, T. J. Bartley, and C. Silberhorn, A high dynamic range optical detector for measuring single photons and bright light, Opt. Express **27**, 1 (2019).

[52] I. Esmaeil Zadeh, J. Chang, J. W. N. Los, S. Gyger, A. W. Elshaari, S. Steinhauer, S. N. Dorenbos, and V. Zwiller, Superconducting nanowire single-photon detectors: A perspective on evolution, state-of-the-art, future developments, and applications, Appl. Phys. Lett. **118**, 190502 (2021).

[53] W. Martienssen and E. Spiller, Coherence and fluctuations in light beams, Am. J. Phys. **32**, 12 (1964).

[54] J. Sperling, W. Vogel, and G. S. Agarwal, Sub-binomial light, Phys. Rev. Lett. **109**, 9 (2012).

[55] P. Grangier, G. Roger, and A. Aspect, Experimental evidence for a photon anticorrelation effect on a beam splitter: A new light on single-photon interferences, Europhys. Lett. **1**, 4 (1986).

[56] R. Filip and L. Mišta, Detecting quantum states with a positive Wigner function beyond mixtures of Gaussian states, Phys. Rev. Lett. **106**, 200401 (2011).

[57] L. Mandel, Sub-Poissonian photon statistics in resonance fluorescence, Opt. Lett. **4**, 205 (1979).

[58] E. J. O'Reilly and A. Olaya-Castro, Non-classicality of the molecular vibrations assisting exciton energy transfer at room temperature, Nat. Commun. **5**, 1 (2014).

[59] B. K. Park, Y.-S. Kim, Y.-W. Cho, S. Moon, and S.-W. Han, Arbitrary configurable 20-channel coincidence counting unit for multi-qubit quantum experiment, Electronics **10**, 5 (2021).